Alzheimer's & Dementia: Translational Research & Clinical Interventions 3 (2017) 481-486

Short Report

Measuring brain synaptic vesicle protein 2A with positron emission tomography and [^{18}F]UCB-H

Mohamed Ali Bahri[a], Alain Plenevaux[a], Joël Aerts[a], Christine Bastin[a], Guillaume Becker[a], Joël Mercier[b], Anne Valade[b], Tim Buchanan[b], Nathalie Mestdagh[b], Didier Ledoux[c], Alain Seret[a], André Luxen[a], Eric Salmon[a,*]

[a]*GIGA-Cyclotron Research Center, University of Liège, Liege, Belgium*
[b]*UCB Biopharma SPRL, Brussels, Belgium*
[c]*Service des soins intensifs généraux, CHU Liege, Liege, Belgium*

Abstract

Introduction: Brain distribution of synaptic vesicle protein 2A was measured with fluorine-18 UCB-H ([^{18}F]UCB-H) and positron emission tomography (PET).

Methods: Images of synaptic density were acquired in healthy volunteers (two young participants and two seniors). Input function was measured by arterial blood sampling (arterial input function) and derived from PET images using carotid activity (image-derived input function). Logan graphical analysis was used to estimate regional synaptic vesicle protein 2A distribution volume.

Results: [^{18}F]UCB-H uptake was ubiquitous in cortical and subcortical gray matter. Arterial input function and image-derived input function provided regional distribution volume with a high linear relationship.

Discussion: The cerebral distribution of [^{18}F]UCB-H is similar to that recently observed with carbon-11 UCB-J ([^{11}C]UCB-J). An accurate [^{18}F]UCB-H quantification can be performed without invasive arterial blood sampling when no suitable reference region is available, using dynamic PET carotid activity. Brain synaptic density can be studied in vivo in normal and pathological aging.

Keywords: SV2A; Neuroimaging; Synapse density; Fluorine-18; PET; Alzheimer's disease

1. Introduction

Alzheimer's disease (AD) is characterized by abnormal brain deposits of amyloid β and neurofibrillary tangles with hyperphosphorylated tau and by loss of synapses [1]. There is a complex relationship between brain protein processing and synaptic functioning [2]. New AD models suggest that abnormal protein deposits and synaptic dysfunction occur many years before AD dementia is diagnosed [3,4]. Different neuroimaging measurements are taken as biomarkers in AD models. Yet a reliable neuroimaging measure of synaptic loss is still needed.

Synaptic vesicle protein 2A (SV2A) is a glycoprotein present in the membranes of most brain synaptic vesicles. Its physiological role is still debated [5]. SV2A is the therapeutic target of levetiracetam, an antiepileptic drug modifying the natural course of epilepsy in several models [6]. The role of SV2A in AD is particularly interesting. SV2A has been found to be reduced postmortem in the hippocampal structures of patients with dementia [7]. Levetiracetam restored dysfunctional networks in a mouse model of AD [8]. Moreover, it improved cognition and decreased hippocampal hyperactivity in patients in the predementia stage of AD [9].

[^{18}F]UCB-H is an original biomarker showing binding specificity for SV2A ([10,11]; Supplementary Data). In a

*Corresponding author. Tel.: + 32 (0)4 366 2316; Fax: + 32 (0)4 366 29 46.
E-mail address: eric.salmon@ulg.ac.be

http://dx.doi.org/10.1016/j.trci.2017.08.004

rat microPET (micro positron emission tomography) study, the total distribution volume (*Vt*) of [^{18}F]UCB-H in the brain was calculated and the test-retest reproducibility was about 10% [11]. Levetiracetam induced dose-dependent blocking and displacement of cerebral [^{18}F]UCB-H uptake. Radiodosimetry was performed in mice [12] and humans [13]. In this study of [^{18}F]UCB-H in healthy volunteers, we characterized its blood-brain pharmacokinetics. SV2A is a suitable marker of synaptic density, and we discuss its brain distribution and modeling properties compared to the recently published SV2A tracer [^{11}C]UCB-J [14]. SV2A is ubiquitous in the brain. There is no "reference region" without binding sites for [^{18}F]UCB, and an arterial blood input function (arterial input function [AIF]) is required for quantifying regional distribution of the radiotracer. An original method using image-derived carotid artery activity is shown to be comparable to classical modeling with AIF.

2. Methods

2.1. Participants

Two young (38 and 46 years) and two senior (66 and 69 years) healthy male volunteers participated in this study (EudraCT 2011-003413-42). Subjects' suitability for participation was determined by interview, physical examination, clinical blood laboratory tests, 12-lead electrocardiogram, and urine drug screening (see Supplementary Data for inclusion/exclusion criteria). The study was approved by the Ethics Committee of Liege University Hospital (Belgium). All participants signed an informed consent form.

2.2. Image acquisition

Dynamic PET acquisitions were performed using a Siemens/CTI (Knoxville, TN) ECAT HR+ PET scanner. About 170.4 ± 24.9 MBq of [^{18}F]UCB-H was injected as an intravenous bolus. The timeframe of the dynamic PET was 6 × 10, 8 × 30, 5 × 120 and 17 × 300 seconds, resulting in 100-minutes scanning time. All PET images were reconstructed using filtered backprojection including corrections for measured attenuation, dead time, random events, and scatter using standard software (ECAT 7.1, Siemens/CTI, Knoxville, TN). A structural magnetic resonance imaging (MRI) image acquired for each subject a few days before PET study (3–10 days) was used to exclude any brain abnormality and to facilitate coregistration of PET data to the standard Montreal Neurological Institute space for brain structures segmentation. MRI data were acquired on a 3T Allegra Siemens scanner (three-dimensional modified driven equilibrium Fourier transform [MDEFT] sequence) with the following parameters: TR = 7.92 ms, TE = 2.4 ms, TI = 910 ms, FA = 15°, FOV = 256 × 224 × 176 mm^3, and isotropic spatial resolution = 1 mm.

2.3. Image quantification

In our analysis plan, we first searched for a suitable input function (IF), and we then searched for a suitable modeling approach.

To measure AIF, blood samples were collected through a cubital artery cannula. AIF was obtained by correcting plasma data for the unchanged tracer fraction determined using high performance liquid chromatography ([11]; Supplementary Data).

However, an arterial cannula cannot be used to study patient cohorts. Since brain SV2A is ubiquitous, it is improbable that a suitable reference region can be found to model radiotracer distribution. Here, we derived IF from dynamic PET images (image-derived input function [IDIF]) using the method described by Schain et al. [15]. The method extracts time series of [^{18}F]UCB-H in the carotid artery by identifying voxels belonging to the carotid. This is based on the computation of the Pearson product-moment correlation coefficient between a "seeding region" (a group of voxels in the carotid) and voxels in a mask containing the carotid (except those used as the seeding region). The extracted time series (IDIF) was then scaled to plasma radioactivity using the last three blood samples and corrected using mean unchanged plasma fractions. The detailed method is reported as Supplementary Data.

PET data were processed with SPM12 (Wellcome Department of Cognitive Neurology, London, UK). For each subject, PET dynamic frames were corrected for movement. The structural MRI image was coregistered to its PET image (sum of the dynamic data) without reslicing. The resulting MRI image was segmented and normalization transformation parameters (forward and inverse: transformation parameters used to bring images to the Montreal Neurological Institute stereotactic space) were calculated. The inverse transformation was used to bring the Automated Anatomical Labeling (AAL) human brain atlas into the PET subject space and extract the time activity curves of all AAL brain atlas regions. Kinetic modeling using both AIF and IDIF was done with PMOD (Version 3.7, PMOD Technologies, Zurich, Switzerland). Since the AAL atlas did not contain white matter (WM) regions, a centrum semiovale region was created using SPM WM probability map. This map was thresholded (>99.6%) to obtain only voxels with the highest WM membership.

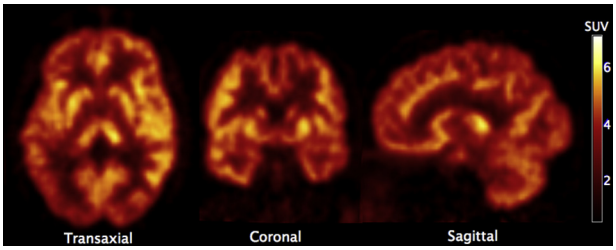

Fig. 1. PET image of the synaptic vesicle protein 2A (SV2A)–specific tracer [^{18}F]UCB-H in a healthy volunteer (average of dynamic images: subject 1, young participant). Radioactivity expressed as standardized uptake value (SUV, normalized to the injected dose and body weight).

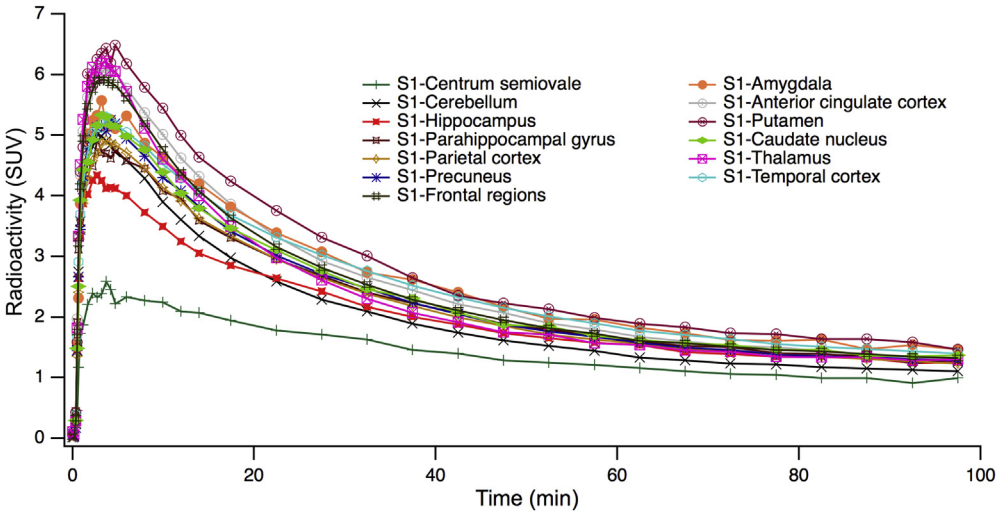

Fig. 2. Time activity curves (TACs) for the selected brain regions of subject 1 (mean left and right hemispheres). Activity expressed as standardized uptake value (SUV).

2.4. Statistical analyses

The similarity between AIF and IDIF was assessed by comparing the area under the curve, searching for a ratio around 1. Moreover, IFs were also fitted using a biexponential model, and the slopes of the IFs were compared using a nonparametric Wilcoxon test. Three kinetic models, 1-tissue compartment (1TC), 2-tissue compartment (2TC), and Logan graphical analysis were used to calculate the *Vt* of [^{18}F]UCB-H in the brain. The three models were compared in terms of stability of estimate over regions (whether the model can fit all regions without failure) and the accuracy of the experimental data fitting (goodness-of-fit: R^2; visual comparison: how close the model curve is to the measurement).

3. Results

PET images averaged over 100 minutes (Fig. 1) revealed a heterogeneous but ubiquitous tracer uptake in subcortical and cortical gray matter regions. [^{18}F]UCB-H brain kinetics were rapid, with an initial high uptake and a standardized uptake value peak (expressed as brain activity normalized to injected dose and body weight) of 5 to 10 across brain regions 10 minutes after injection, followed by rapid decline in regional radioactivity over time (Fig. 2).

Blood data analysis showed a consistent tracer amount in whole blood and plasma indicating low binding to red blood cells. Unchanged [^{18}F]UCB-H fraction in plasma followed a 3-exponential decrease with a starting fraction of 97 ± 2% (mean ± SD) measured 3 minutes after injection. This fraction was subsequently measured at 5, 15, 35, 60, and 90 minutes and decreased to 85 ± 17%, 37 ± 14%, 30 ± 13%, 21 ± 8%, and 17 ± 8%, respectively. Scaled IDIF was found to be very similar to AIF, with a mean ratio of area under the curve of 1.02 ± 0.08. This was true for plasma and whole blood AIF (Table 1). Moreover, the comparison of slope constants of the biexponential fit for the IFs, which provide an indication of the instantaneous level of blood radioactivity,

Table 1
Area under the curve ratio between manual blood sampling and image-derived carotid blood activity

	Subjects						
Variables	S1 AUCr	S2 AUCr	S3 AUCr	S4 AUCr	Mean	SD	COV
Unfitted IF							
Plasma/IDIF	0.981	0.923	1.119	1.051	1.018	0.085	8.342
MFB/IDIF	0.944	0.968	1.053	0.984	0.987	0.047	4.752
Fitted IF							
Plasma/IDIF	1.068	0.978	0.934	1.049	1.008	0.062	6.189
MFB/IDIF	1.031	1.009	0.907	1.006	0.988	0.055	5.599

Abbreviations: AUCr, area under the curve ratio; COV, coefficient of variation; IF, input function; IDIF, image-derived IF scaled to three plasma last samples; MFB, measured full blood activity; plasma, measured plasma activity; S1 to S4, participants; SD, standard deviation.

Table 2
Biexponential fit slope constants for manually sampled and image-derived input functions

	Subjects					
Variables	S1	S2	S3	S4	Mean	SD
Slope 1						
MFB	2.268	2.521	3.575	6.096	3.615	1.748
Plasma	2.116	2.518	3.846	6.250	3.683	1.864
IDIF	1.805	1.619	3.432	4.113	2.742	1.224
Slope 2						
MFB	0.003	0.009	0.031	0.010	0.013	0.012
Plasma	0.002	0.010	0.034	0.010	0.014	0.014
IDIF	0.002	0.009	0.010	0.007	0.007	0.004

Abbreviations: IDIF, image-derived input function scaled to last three plasma samples; MFB, measured full blood activity; plasma, measured plasma activity; S1 to S4, participants; SD, standard deviation.

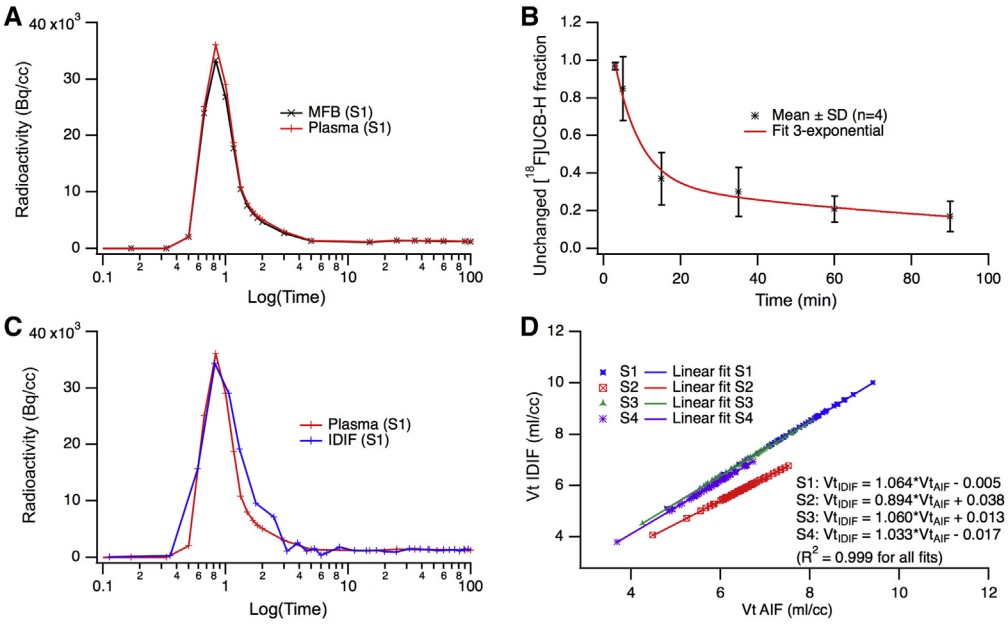

Fig. 3. Input function (IF) evaluation for [^{18}F]UCB-H tracer: (A) [^{18}F]UCB-H in blood (MFB, measured full blood) and in plasma (S1, subject 1). Radioactivity in Becquerel per cubic centimeter (Bq/cc); (B) Mean unchanged [^{18}F]UCB-H in plasma for the four participants. SD, standard deviation; (C) Image-derived input function (IDIF) scaled to match the plasma measures using the last three plasma values and measured plasma IF (plasma; subject 1); (D) Scatter plot representing distribution volumes obtained with image-derived IF (Vt_{IDIF}) versus distribution volumes obtained with arterial IF (Vt_{AIF}). S1 to S4 are participants. Distribution volumes were estimated using the Logan graphical analysis method for all Automated Anatomical Labeling brain atlas regions. We could not find any clinical or paraclinical information to explain the difference between S2 and the other volunteers.

showed similar values for AIF and IDIF, especially for the second slope constant ($Z = 1.82$, $P > .06$; Table 2).

The three kinetic models (1TC, 2TC, and Logan) led to a consistent estimation of *Vt*. The 1TC gave a weak fitting of the data (measurement did not lie on the model curve, R^2: 0.95), whereas the 2TC model fitted the data well (R^2: 0.98) and provided total and specific values for distribution volume of the tracer, but not for all regions (few failures to fit experimental data). In contrast, Logan graphical model provided reliable *Vt* estimates with suitable fits (R^2: 0.99) and reasonable start time (t* ranged between 15 and 30 minutes). Thus, Logan graphical model was chosen as the preferential method for analysis of the data using both AIF and IDIF and with a t* of 25 minutes (mean value over all regions and subjects). An estimate of the IF delay was included in the model to optimize its fit. A high linear relationship ($R^2 > 0.99$; slope: 1.013 ± 0.080) was observed between *Vt* values obtained with AIF and IDIF (Fig. 3). Mean *Vt* values ranged from 4.3 mL/cm^3 in the centrum semiovale to 7.8 mL/cm^3 in the gyrus rectus for both AIF and IDIF analyses. The single reserve was that *Vt* coefficients of variation were moderately higher for IDIF (17± 2%) than for AIF analysis (12 ± 2%). Supplementary Fig. 1 depicts regional *Vt* in the left cerebral hemisphere. *Vt* showed increasing values from the WM to the cerebellum, hippocampus, parahippocampal gyrus, parietal cortex, precuneus, frontal regions, amygdala, anterior cingulate cortex, and putamen (Fig. 4). Referring to Finnema et al.'s study with

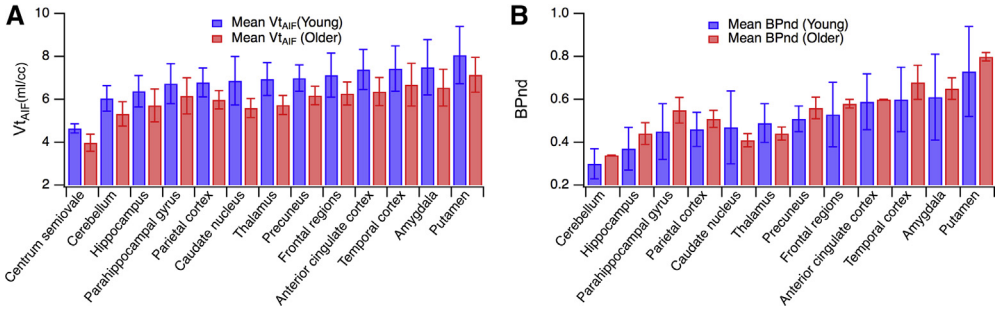

Fig. 4. PET quantitative data of [^{18}F]UCB-H tracer in a healthy human brain: (A) regional volumes of distribution (*Vt* in mL per cubic centimeter) obtained by the Logan graphical analysis model applied to time-activity curves using arterial input function (AIF, means ± SD, n = 2 for each group); (B) BP_{ND} values (binding potential calculated using centrum semiovale region with "nondisplaceable" activity) calculated as $Vt_{(region)}/Vt_{(centrum\_semiovale)} - 1$.

[^{11}C]UCB-J [14], we calculated binding potential (BP_{ND}) using WM as pseudo-reference (representing nondisplaceable free and nonspecific binding). Unexpectedly, older participants had a higher BP_{ND} than younger ones (Fig. 4).

4. Discussion

[^{18}F]UCB-H has been used as a biomarker for SV2A [11]. A recent publication using [^{11}C]UCB-J (a similar derivative of levetiracetam) showed a correlation between in vivo brain radiotracer binding and postmortem measures of brain SV2A in a baboon study [14]. Full quantification of [^{18}F]UCB-H binding through kinetic modeling was possible in the absence of a reference region devoid of specific tracer binding [16]. [^{18}F]UCB-H was shown to have negligible amount of radiometabolites in the rat brain [17]. Although [^{18}F]UCB-H uptake observed in WM is relatively low, making it a candidate for a reference region in young people [14], WM is altered by AD [18,19], calling into question the value of WM as a pseudo-reference for older participants. Moreover, [^{18}F]UCB-H binding in pons was displaced with levetiracetam at 10 mg/kg in rats [11]. Therefore, an image-derived carotid signal was preferred as the IF for complete kinetic modeling. The IDIF result closely matched the result derived by manual arterial blood sampling (the "gold standard").

[^{18}F]UCB-H brain uptake confirmed the ubiquitous cerebral distribution of SV2A [11,14,20]. A Logan graphical model was used to describe brain accumulation, whereas a 1TC was chosen for modeling [^{11}C]UCB-J [14]. Although the two tracers are quite similar, *Vt* values are higher with [^{11}C]UCB-J (5–22 ml/cc) than with [^{18}F]UCB-H (3–10 ml/cc), whereas [^{18}F]UCB-H has a longer half-life for performing population studies. Investigation of [^{18}F]UCB-H distribution in medial temporal structures, the default mode network, and the anterior cingulate cortex would be particularly interesting to explore the temporal relationship between brain amyloid and tau pathology and brain synaptic loss in AD [4,21] or study frontotemporal dementia [22].

Owing to the demanding PET protocol (arterial blood sampling, very selective inclusion criteria), only four subjects were recruited for this study. The mean parent fraction was used to correct IFs for metabolites, and this profile should be measured in venous blood for different patient groups. The time activity curves suggest that scan duration, another limitation, might be reduced to 50 minutes while retaining appropriate "Logan-modeling" properties. Finally, image correction for partial volume effects should be discussed in any patient study.

In conclusion, our results suggest that [^{18}F]UCB-H is a good candidate as radiotracer for brain SV2A and can be used for human studies. IDIF was showed to be useful for quantitative studies without the need to arterial blood sampling.

Acknowledgments

The authors thank Dr E.Z. for providing Python scripts to create Supplementary Fig. 1.
This work was funded by the Walloon Region Public Private Partnership NeuroCom, with the University of Liege and UCB Pharma as partners. Analyses benefited from grants from a Belgian Interuniversity Attraction Pole (IUAP 7/11) and from ULg Research Concerted Action (ARC 12/17-01). A.P. is a research director and C.B. is a research associate at the FRS-FNRS Belgium.

Supplementary data

Supplementary data related to this article can be found at http://dx.doi.org/10.1016/j.trci.2017.08.004.

RESEARCH IN CONTEXT

1. Systematic review: Brain synapses can be measured using a PET radiotracer specific to synaptic vesicle protein 2A (SV2A). [^{18}F]UCB-H brain distribution was quantified in healthy volunteers and compared to recently published data on [^{11}C]UCB-J.
2. Interpretation: SV2A was seen in all subcortical and cortical cerebral gray matter structures. Temporal structures were particularly well delineated with [^{18}F]UCB-H as with [^{11}C]UCB-J. Volumes of distribution could be obtained using an input function derived from PET dynamic activity in carotid, with results similar to a standard arterial blood input function.
3. Future directions: [^{18}F]UCB-H is suitable to noninvasively explore human brain synaptic density in normal and pathological conditions, such as very early Alzheimer's disease.

References

[1] Hyman BT, Phelps CH, Beach TG, Bigio EH, Cairns NJ, Carrillo MC, et al. National Institute on Aging-Alzheimer's Association guidelines for the neuropathologic assessment of Alzheimer's disease. Alzheimers Dement 2012;8:1–13.
[2] Spires-Jones TL, Hyman B. The Intersection of amyloid beta and tau at synapses in Alzheimer's disease. Neuron 2014;82:756–71.
[3] Pozueta J, Lefort R, Shelanski ML. Synaptic changes in Alzheimer's disease and its models. Neuroscience 2013;251:51–65.
[4] Jack CR, Holtzman DM. Biomarker modeling of Alzheimer's disease. Neuron 2013;80:1347–58.
[5] Mendoza-Torreblanca JG, Vanoye-Carlo A, Phillips-Farfán BV, Carmona-Aparicio L, Gómez-Lira G. Synaptic vesicle protein 2A: Basic facts and role in synaptic function. Eur J Neurosci 2013;38:3529–39.
[6] Lynch BA, Lambeng N, Nocka K, Kensel-Hammes P, Bajjalieh SM, Matagne A, et al. The synaptic vesicle protein SV2A is the binding

site for the antiepileptic drug levetiracetam. Proc Natl Acad Sci U S A 2004;101:9861–6.

[7] Robinson JL, Molina-Porcel L, Corrada MM, Raible K, Lee EB, Lee VM, et al. Perforant path synaptic loss correlates with cognitive impairment and Alzheimer's disease in the oldest-old. Brain 2014; 137:2578–87.

[8] Sanchez PE, Zhu L, Verret L, Vossel KA, Orr AG, Cirrito JR, et al. Levetiracetam suppresses neuronal network dysfunction and reverses synaptic and cognitive deficits in an Alzheimer's disease model. Proc Natl Acad Sci 2012;109:E2895–903.

[9] Bakker A, Krauss GL, Albert MS, Speck CL, Jones LR, Stark CE, et al. Reduction of hippocampal hyperactivity improves cognition in amnestic mild cognitive impairment. Neuron 2012;74:467–74.

[10] Mercier J, Archen L, Bollu V, Carré S, Evrard Y, Jnoff E, et al. Discovery of heterocyclic nonacetamide synaptic vesicle protein 2A (SV2A) ligands with single-digit nanomolar potency: opening avenues towards the first SV2A positron emission tomography (PET) ligands. ChemMedChem 2014;9:693–8.

[11] Warnock GI, Aerts J, Bahri MA, Bretin F, Lemaire C, Giacomelli F, et al. Evaluation of 18F-UCB-H as a novel PET tracer for synaptic vesicle protein 2A in the brain. J Nucl Med 2014;55:1336–42.

[12] Bretin F, Warnock G, Bahri MA, Aerts J, Mestdagh N, Buchanan T, et al. Preclinical radiation dosimetry for the novel SV2A radiotracer [18F]UCB-H. EJNMMI Res 2013;3:35.

[13] Bretin F, Bahri MA, Bernard C, Warnock G, Aerts J, Mestdagh N, et al. Biodistribution and radiation dosimetry for the novel SV2A radiotracer [18 F]UCB-H: first-in-human study. Mol Imaging Biol 2015; 17:557–64.

[14] Finnema SJ, Nabulsi NB, Eid T, Detyniecki K, Lin SF, Chen MK, et al. Imaging synaptic density in the living human brain. Sci Transl Med 2016;8:348ra96.

[15] Schain M, Benjaminsson S, Varnäs K, Forsberg A, Halldin C, Lansner A, et al. Arterial input function derived from pairwise correlations between PET-image voxels. J Cereb Blood Flow Metab 2013; 33:1058–65.

[16] Lammertsma AA, Hume SP. Simplified reference tissue model for PET receptor studies. Neuroimage 1996;4:153–8.

[17] Becker G, Warnier C, Serrano ME, Bahri MA, Mercier J, Lemaire C, et al. Pharmacokinetic Characterization of [18F]UCB-H PET Radiopharmaceutical in the Rat Brain. Mol Pharm 2017;14:2719–25.

[18] Brun A, Englund E. A white matter disorder in dementia of the Alzheimer type: A pathoanatomical study. Ann Neurol 1986;19:253–62.

[19] Rieckmann A, Van Dijk KR, Sperling RA, Johnson KA, Buckner RL, Hedden T. Accelerated decline in white matter integrity in clinically normal individuals at risk for Alzheimer's disease. Neurobiol Aging 2016;42:177–88.

[20] Bajjalieh SM, Frantz GD, Weimann JM, McConnell SK, Scheller RH. Differential expression of synaptic vesicle protein 2 (SV2) isoforms. J Neurosci 1994;14:5223–35.

[21] Dubois B, Hampel H, Feldman HH, Scheltens P, Aisen P, Andrieu S, et al. Preclinical Alzheimer's disease: definition, natural history, and diagnostic criteria. Alzheimers Dement 2016;12:292–323.

[22] Zhou J, Greicius MD, Gennatas ED, Growdon ME, Jang JY, Rabinovici GD, et al. Divergent network connectivity changes in behavioural variant frontotemporal dementia and Alzheimer's disease. Brain 2010;133:1352–67.